DETECTION AND INTERPRETATION OF OCEAN ROUGHNESS VARIATIONS ACROSS THE GULF STREAM INFERRED FROM RADAR CROSS SECTION OBSERVATIONS

D. E. Weissman
Dept. of Engineering and
Computer Sciences
Hofstra University
Hempstead, New York 11550
and
Jet Propulsion Laboratory
Pasadena, Calif. 91103

T. W. Thompson
Planetary Science Institute
Science Applications, Inc.
Pasadena, Calif. 91101
and
Jet Propulsion Laboratory
Pasadena, Calif. 91103

Abstract

During the past several years, many radars have observed the distinct and interesting features associated with the Gulf Stream and its boundaries. Some of these Gulf Stream radar features have small scale, with dimensions comparable to and slightly greater than long gravity waves. Other features are larger, with dimensions much greater than the length of long gravity waves. This study describes radar cross section variations within the Gulf Stream and just outside, seen with a "scatterometer" type measurement.

The significant features of this radar cross section data were that the Gulf Stream always had a higher cross section per unit area (interpreted here as a greater roughness) than the water on the continental shelf. Also, a steep gradient in cross section was often seen at the expected location of the western boundary. There were also longer scale (10 to 20 km) gradual fluctuations within the stream of significant magnitude. These roughness variations are correlated with the surface shear stress that the local wind imposes on the sea. Using the available surface truth information regarding the wind speed and direction, an assumed Gulf Stream velocity profile, and high resolution ocean surface temperature data obtained by the Very High Resolution Radiometer onboard a NOAA-NESS polar-orbiting satellite (data provided by Dr. Richard Legeckis of NOAA-NESS), this study demonstrates that the computed surface stress variation bears a striking resemblence to the measured radar cross-section variations.

1. Introduction

The western boundary of the Gulf Stream has the unusual property of generating strong features (both small and large scale) in radar images. An imaging radar detection of the Gulf Stream in 1972 was reported by Moskowitz [1]. These showed large spatial scale and small-scale (narrow filaments) cross-section variations that are independent of the wave imaging characteristics. Also, radar altimetry (at 13.9 GHz) from aircraft and observations from the GEOS-3 and Skylab spacecraft have revealed definite differences in the radar cross section between the Gulf Stream and the continental shelf. Published data and quantitative analysis of these observations are very limited [2].

The Marineland Test [3], conducted during the first half of December 1975, provided new data on these Gulf Stream radar features. In particular, this test employed the JPL[1] and ERIM[2] airborne synthetic aperture imaging radars (SAR) and several surface instruments. All five flights of the JPL L-Band observed significant variations and oscillations of the surface radar cross section as detected by a "scatterometer" measurement mode. This scatterometer mode of measurement led to some unanticipated observations: the Gulf Stream often has a significantly higher radar cross-section (per unit area) than the water on the continental shelf between shore and the continental slope. These differences are often accompanied by large-scale (spatial) variations near the boundary. This report will concentrate on these variations. The primary data for this effect is the strip chart record of the received power history that was kept continuously on a selected flight line. Comparisons will often be made between the strip chart recording and the features observed simultaneously in the SAR images. Also, infrared satellite photographs (obtained by the very high resolution radiometer on the NOAA-NESS satellite), optical photos taken from the CV-990, and other sources of related information have been examined whenever available.

Much of the interpretation of our data is based on the concept of a Bragg scattering, where radar echo strength is determined by the number of ocean waves which have crests aligned with radar's line of sight and have crest-to-crest spacing which is equal to one-half of the peak-to-peak spacing of the electromagnetic radiation [4]. Thus, the L-band radar with 25-cm wavelength basically observes the population of ocean waves which have wavelengths of [12.5 cm/sin (angle of incidence)] and have directions directly toward or away from the aircraft. For simplicity, the ocean waves with these wavelengths and directions will be called the "Bragg waves."

The Bragg surface wavelength is actually one value in a continuous spectrum of the randomly rough surface. The strength (radar cross section per unit area) of the signal backscattered by a small patch of the ocean (say a resolution cell of the SAR) will be proportional to the local number of short gravity waves of the proper length and directional alignment, and their maximum heights. The modulation of these shorter waves by the large gravity waves is the basis for the scattering differences observed as waves in a radar image. In the scatterometer mode described below, only the total cross section integrated across the large illuminated area (see Fig. 2) is being observed, at any instant. This provides an observation of the average "density" of Bragg wavelengths and is interpreted as the degree of roughness of the

[1]Jet Propulsion Laboratory

[2]Environmental Research Institute of Michigan

illuminated area. The physical quantity that controls these populations of Bragg waves is the wind stress.

The scatterometer measurements were also compared with the synthetic aperture radar images. The relationship between the effects seen on the strip chart and the image is generally complex. There are large differences between the spatial scales of cross-section variations observed with these two techniques. The strip chart measurement method is more sensitive to changes in cross-section magnitude as small as a few tenths of a dB, whereas the radar image gives very precise location, alignment, and finer spatial size information. Also, the separate flights will be analyzed separately because of the different character of the observed effects and because of the availability or lack of the infrared satellite data.

Observed radar cross sections were found to be correlated with an estimated surface stress. Surface stress estimates accounted for surface winds, differential modulation of the surface wind by the Gulf Stream, and air-sea temperature differences. Surface winds were measured by surface instruments at the Marineland Test sites, and we assumed that these were uniform everywhere in the test area. The Gulf Stream surface velocity was modelled, with a profile published earlier by Von Arx [5]. Sea temperatures were estimated from VHRR (Very High Resolution Radiometer) data provided by Dr. Richard Legeckis of NOAA-NESS. Air temperatures were given by the surface instruments. The sea temperatures given by the VHRR provided a substantial improvement over sea temperatures estimated in our earlier report [6].

These estimated surface stresses were compared with the radar backscatter data for December 4 and 15, 1975 (other days weren't studied, since the Marineland Test area was under clouds, preventing the acquisition of surface temperature information). These results show that both large scale trends (over a range of 250 km) and small scale features (on the order of tens of kilometers) in the radar data correlates extremely well with the square root of the computed surface stress.

The results presented here imply that the backscattered radar cross section measured by the radar is proportional to the surface stress which is seen to be a function of the local wind, the surface current, and the surface temperature. If the distribution of two of these quantities can be measured or estimated, then the third can be inferred, using the measurement technique and interpretation discussed in the following. Further evidence that sea-air temperature differences should be considered along with the wind and current interaction can be found in some recent cross-section measurements (from nadir) across the Gulf Stream made by the SKYLAB altimeter. This data shows that a variety of effects is observable, indicating a sensitivity to the meteorological conditions. The data analyzed by Parsons [2] cannot be fully explained by just considering the wind vector and the local current information. This implies that surface temperature influences the surface roughness.

2. Instruments and Flight Patterns

Imaging Radar

The radar data presented here was obtained in five flights of the JPL L-Band imaging radar onboard the NASA CV-990.[3] The data is basically scatterometry, where radar echo strength in terms of a backscatter radar cross section per unit area of the surface is measured. The variations of radar echo are monitored along a ground track parallel to the aircraft's line of flight. Also, radar echo strengths are provided by two different but simultaneous modes. The normal imaging mode records the full signal information on a signal film recorder on board the aircraft. After the flight, these signal films are converted to high-resolution images, using an optical correlator. The "scatterometer" mode simply records total received power returning from an area whose spatial width is determined by the azimuthal beamwidth of the antenna (usually 4.0 km) but whose range spread depends on the transmitted pulse width (usually 0.55 km). The incidence angle can be adjusted with the setting of a range gate. The echo strength recorded on a strip chart is real time on board the aircraft.

An overview of the JPL imaging radar, emphasizing both modes of scatterometry, is shown in Figure 1. Parameters are given in Table 1. Echoes from the surface are received and split into two nearly identical receiver chains and recorded on a signal film via the optical recorder. These signal films were developed, and processed in an optical correlator to provide the high-resolution images which can then be scanned by the densitometer to provide fine-scale scatterometry. Coarse-scale scatterometry was provided by a chain of electronics which sampled the echo at a specified delay, integrated the voltage, and then recorded the result on a strip chart. This provided a continuous record of the relative changes in the total received power from this particular incidence angle.

The geometry of the footprint for strip chart recordings is shown in Fig. 2. The JPL L-Band radar has a large beamwidth antenna (18 deg) which illuminated an area on the right side of the aircraft. This azimuthal beamwidth is aligned perpendicular to the aircraft fuselage. The elevation beamwidth of 90 deg is centered 45 deg above the vertical. A much smaller portion of this antenna footprint is observed by transmitting short pulses and sampling their echoes at a fixed time beyond nadir. Typical parameters for the scatterometer footprint are given in Table 2.

Flight Lines

Radar observations of the Gulf Stream were obtained on five flights in December 1975, when the NASA CV-990 operated out of Patrick AFB in support of the Marineland Test. An overview of these flights is given by Thompson [7]. The positions of some of these flight lines with respect to the Gulf Stream are shown in Fig. 3.

The western boundary of the Gulf Stream in the vicinity of Station III was observed often. The first leg of the Eight-Sided Pattern, was extended out to sea, started at the midpoint of the Gulf Stream and ran in toward shore. All five legs of the Five-Sided Pattern at Station III were centered on a position of 29° 57'N and 80° 17'W at a nominal location of the western boundary. The Gulf Stream Transit started east of the Stream, ran across it, past Station III, and into shore near Station I. The depth profile of the ocean just under the flight path is shown in Figure 4 [14].

Satellite Radiometer

As mentioned above, an important addition to our data base was the sea-surface temperature provided by

[3] The Galileo II, a four jet flying laboratory operated by the Medium Altitude Mission Branch, NASA Ames Research Center.

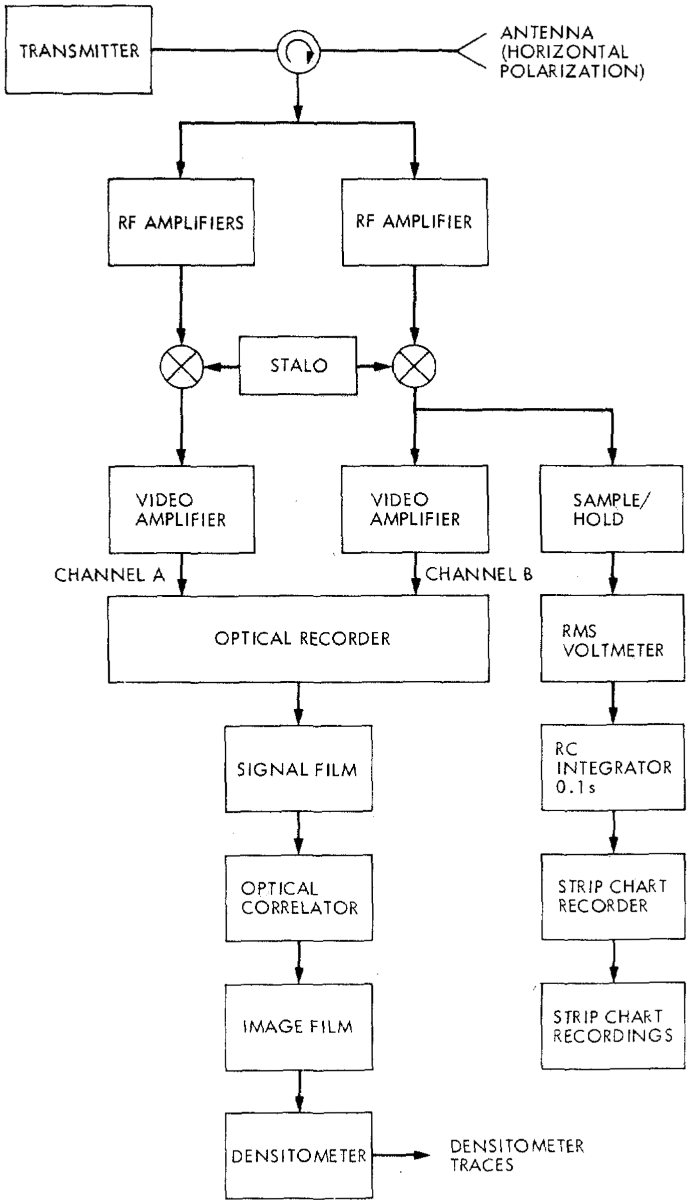

Fig. 1. JPL L-band Radar Block Diagram

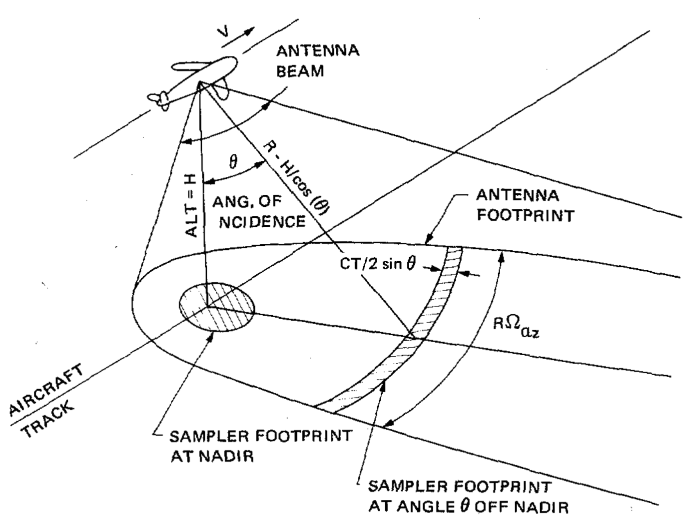

Fig. 2. Surface Illumination Geometry and Parameters

TABLE 1. OPERATING PARAMETERS FOR JPL L-BAND, TWT RADAR

Parameter	Value
Center frequency	1220 MHz
Wavelength	24.6 cm
Pulse length	1.25 μs
Bandwidth	10 MHz
Time-bandwidth product	12.5
Peak power	4 kW
Antenna azimuth beamwidth	18 deg
Antenna range beamwidth	90 deg
Antenna beam center gain	12 dB
Nominal altitude	3 to 12 km
Nominal ground speed	400–500 knots
Sweep time	55 μs
Sweep length	25 mm
Sweep speed	0.44 mm/μs
Range cells	1667
Nominal pulse repetition frequency	800 pps at 400 knots 1000 pps at 500 knots

TABLE 2. TYPICAL VALUES FOR THE STRIP CHART SCATTEROMETER

H	= altitude	= 12 km (40,000 ft)
θ	= angle of incidence	= 20 deg
R	= range	= 12.8 km
Ω_{az}	= azimuth beamwidth	= 18 deg
T_P	= transmitter pulse length	= 1.25 μs
C/2	= velocity of light/2	= 150 m/μs
$R\Omega_{az}$	= azimuth (along-track) footprint length	= 4.0 km
$C\ T_p/2 \sin(\theta)$	= range (cross-track) length	= 0.55 km
Nadir footprint area		= 14.1 km^2
Nadir footprint radius		= 2.1 km
Antenna gain at beam center (θ = 45 deg)		= 12.0 dB
Antenna gain at θ = 20 deg		= 10.5 dB
Antenna gain at nadir		= 7.5 dB

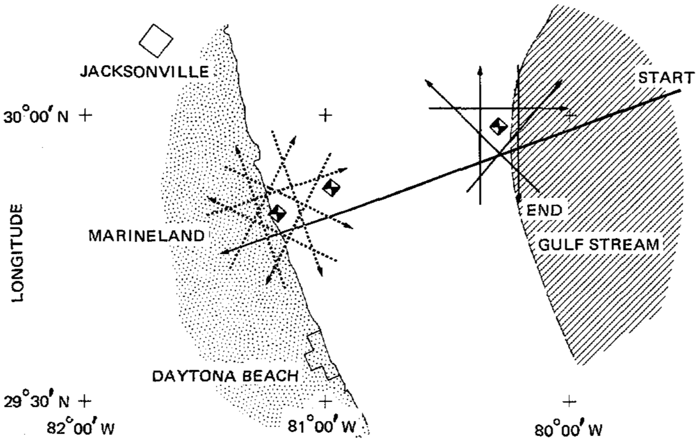

Fig. 3. Flight Paths for Eight-Sided Pattern at Station I and Five-Sided Pattern at Station III

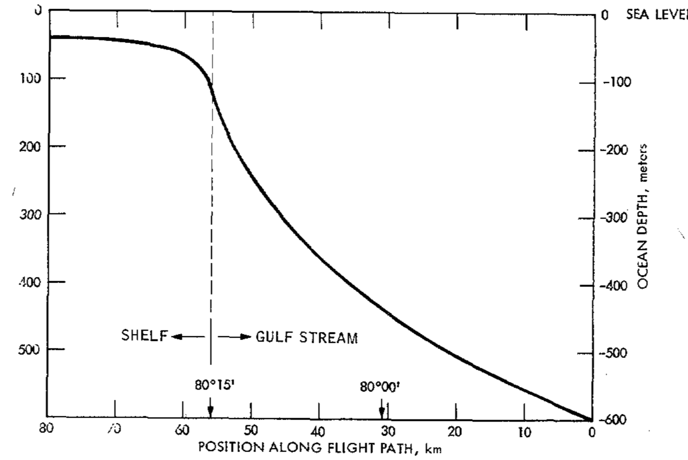

Fig. 4. Ocean Depth Along Flight Path near Gulf Stream Edge, Determined from a Topographic Map [14]

the Very High Resolution Radiometer (VHRR) onboard the NOAA-4 satellite. The VHRR has an instantaneous field of view of about 1 km, and measures radiation in the 0.6 - 0.7 μm (visible) and 10.5 - 12.5 μm (thermal IR) spectral bands. The NOAA-4 spacecraft provides complete day and night coverage of the globe every 24 hours, since it is in a polar orbit at an altitude of about 1500 km. Surface temperature images are constructed from successive scan lines, and the VHRR data can be displayed as gray scale images by using scale values appropriate to the measured radiances. The system sensitivity is about 0.5 to 1.0° C when viewing the ocean surface, and this represents the minimum temperature differential that can be resolved for two adjacent 1 km areas. For larger areas, temperature differences smaller than this can be resolved by suppressing some of the random noise effects by averaging.

The thermal data analyzed here was digitized from the analog transmissions and are presented in the form of quantized sea surface temperature levels (separated by approximately 1.1°), each level representing the temperature within a 2 km square cell. This resolution is comparable to that of the radar cross-section data from the strip chart.

3. Radar Observations During The December 4 Flight

As mentioned previously, the flights on December 4, 1975, provided the best day for correlation of estimated surface stress with radar backscatter from the strip-chart scatterometer. The sea-temperature estimates from the VHRR were acquired at 13:00 GMT, at four and seven hours before the radar data and at 02:00 GMT on December 5, 1977, at four and seven hours after the radar data was acquired. On this day, the strip chart recorder was monitoring the signal that arrived 5 μs after the leading edge, corresponding to a 20-deg incidence angle.

The differences in radar cross section between the Gulf Stream and the adjacent continental shelf waters were 1 to 2 dB. In addition, there were strong oscillations in the cross section near the edge of the stream. These oscillations can be seen in the strip chart data record (Figs. 5a and 6a), where the power levels are normalized such that unity is the minimum backscattered power (or 0 dB) on the continental shelf side of the boundary. The oscillations in the cross section have sizes between 10 and 20 km, which are larger than the resolution size inherent in this technique. These flight lines took place within three hours. Thus, the cross-section behavior with position shows that these 10 to 20 km features are not stationary over this time interval, but that the overall average higher cross section on the Gulf Stream is still evident. A cross correlation between the radar cross section and the computed stress (square root) variations (with means removed) shows a 0.52 correlation for the first Gulf Stream transit and 0.71 for the second. Thus, there is a close relationship between observed radar backscatter and estimated surface stress.

The one-dimensional nature of this strip chart data should be compared with the two-dimensional information in the SAR images. For example, Fig. 7 is the

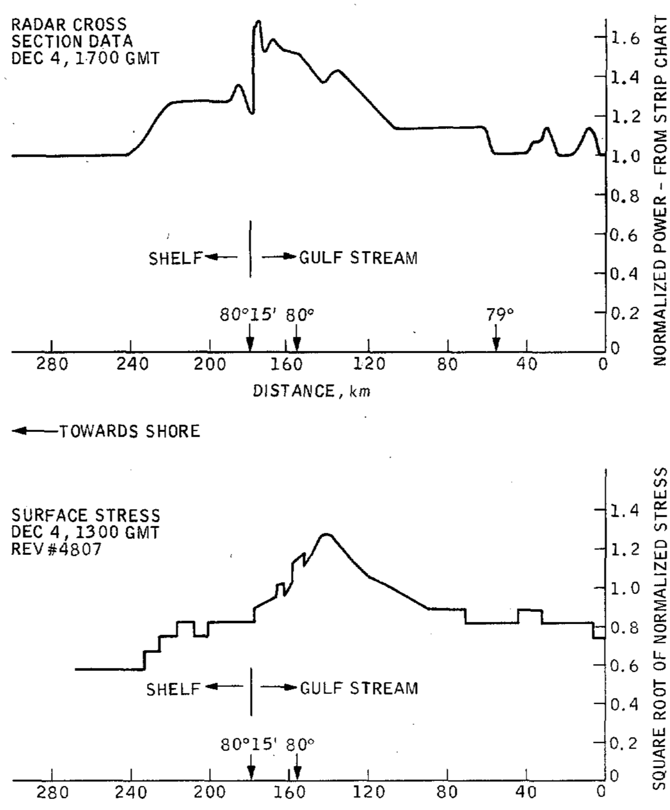

Fig. 5. Comparison between Radar Cross Section Variations and Surface Stress for First Gulf Stream Transit on December 4

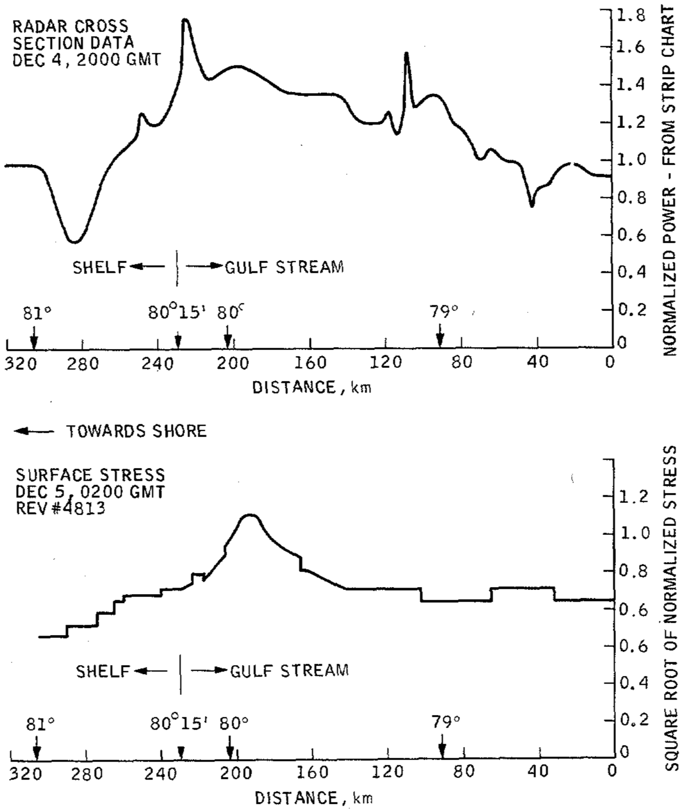

Fig. 6. Comparison between Radar Cross-Section Variations and Surface Stress for Second Gulf Stream Transit on December 4

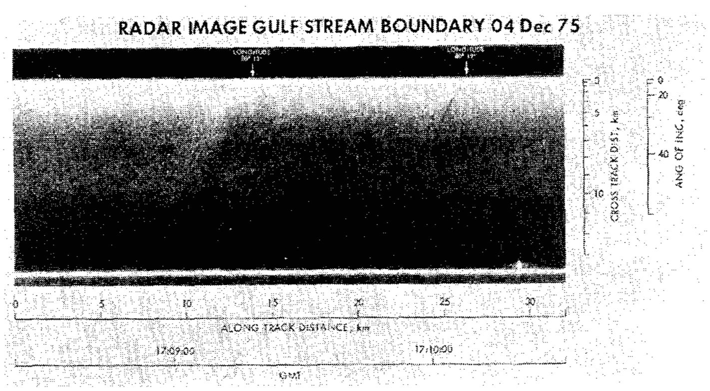

Fig. 7. Synthetic Aperture Radar Image, December 4, 1975 at 17:09:00 GMT

radar image corresponding to the strip chart records of Fig. 5. The linear features in the SAR image display neighboring dark and bright bands of intensity. These features in the image lie approximately parallel to the current flow direction (northerly direction) and to the edge of the Stream. Their positions agree closely with positions where strong changes in cross section were seen in the strip chart record. Moreover, later images of this area show that these linear features maintain their thin appearance for the several hours.

A study of a long record of the radar images (the second Gulf Stream transit) shows similar isolated features in the center of the Stream (for example at 78° 22' longitude, 180 km from western edge). This suggests that the phenomenon is not exclusively associated with the edge of the Stream or the continental slope. Similarly, on different days, other long flight paths will show multiple occurrences of these elongated features.

The features at the Gulf Stream boundary are typically one kilometer wide - too small to be accurately resolved by the scatterometer measurement. Thus, the actual cross-section changes in this thin filament are most likely stronger than those recorded on the strip chart. This record represents an average over a 4.0-km beamwidth. On the other hand, the longer scale undulations in cross section seen with the scatterometer cannot be observed visually from the SAR image, although they might be detectable with image processing.

4. Radar Observations During The December 15 Flight

This last flight of the Marineland Test was also examined in detail because the strip chart recording of cross section had the largest number of oscillations (about 5) and showed the largest maximum to minimum excursion, 2.8 dB for a two-cycle fluctuation extending over a 50-km span (Fig. 8). Once again, the strip chart recorder was operated for a 20-deg incidence angle. The waves over the continental shelf displayed a lower average cross section than the Gulf Stream. It was also noted in the strip chart record that the variations extended much closer to shore than had previously been the case (up to within about 50 km of shore). The extent of the area in which these cross-section variations occur can also be seen in the SAR images. These images indicate that the incidence angle chosen for the strip chart is not critical, and the 20-deg data cited above is a representative sample of similar behavior over a wide range of incidence angles from about 10° to 50° (Fig. 9).

The second Gulf Stream transit of this day yielded an image with a comparable dramatic feature at the edge. The incidence angle used for the accompanying strip

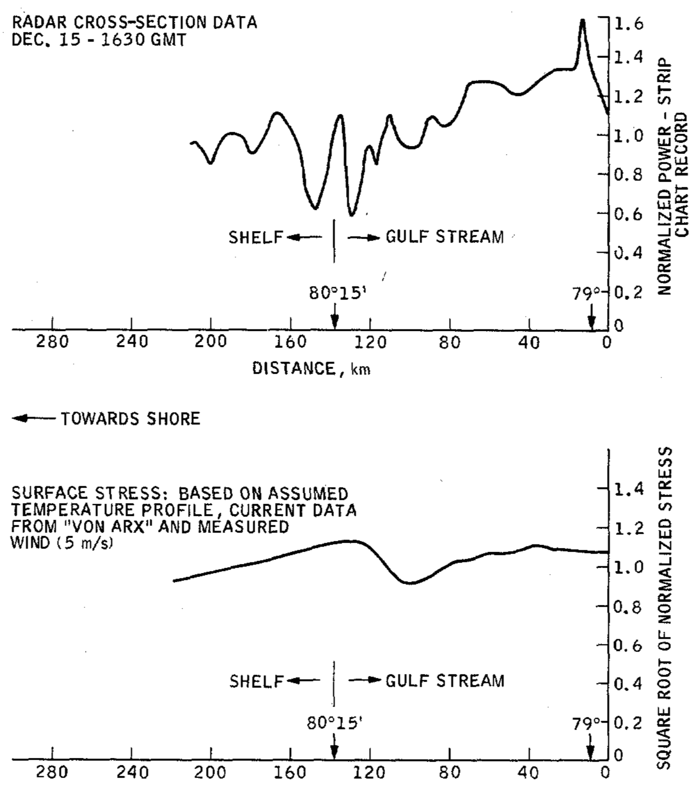

Fig. 8. Comparison between Radar Cross-Section Variations and Assumed Surface Stress for December 15

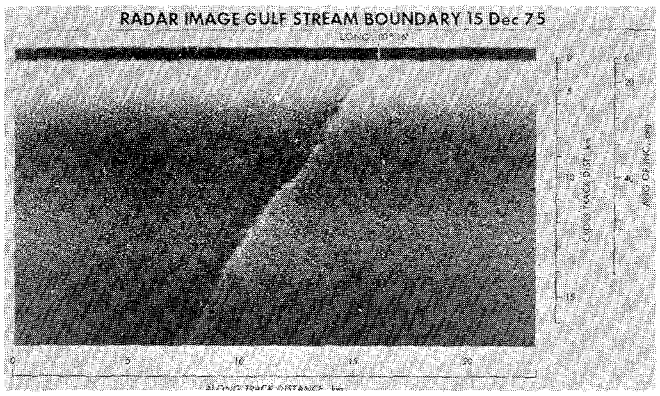

Fig. 9. Synthetic Aperture Radar Image on December 15, 1975 at 16:34:00 GMT

chart record was 0^{o}deg (nadir). Instead of the strong oscillations characteristic of the 20° angle of incidence observations, a much smoother history is seen. The radar observations only show a very gradual increase in cross section as the flight track passes from the Gulf Stream to the continental shelf, amounting to a net change of about 0.5 dB over a distance of about 75 km. This suggests that the ocean phenomena witnessed at off-nadir angles of incidence during the earlier pass with both the imagery and the strip chart record may be affecting the small-scale, Bragg wavelength gravity waves predominantly, and not having much of an effect on the RMS slope (which seems to be a bit higher on the Stream) that controls the nadir radar return.

5. Other Observed Radar Cross-Section Features

One puzzle in these Marineland Test observations is the nature of the thin linear features that are found at the edge of the Stream, and sometimes farther east (Fig. 9). These features probably have stronger cross-section excursions than those recorded on the strip chart. The SAR images show them to have a small width, relative to the width of the area illuminated by the antenna, so their strength would be diluted in the area integration that the antenna performs when the "scatterometer" type of cross-section measurements are made.

Their persistent north-south alignment and extremely narrow dimensions rule out an explanation based on purely temperature variation. It seems unlikely that steep gradients and differences in temperature in such a narrow region (less than 1 km) could be large enough to produce the large roughness difference implied by the observed variations. Based on a detailed optical scan of this feature in a radar image similar to Fig. 9, the temperature excursion would have to be 6°C in order to account for this effect. Also, one would expect some sharp temperature gradients to be aligned in other directions. One suggestion is that these features are related to internal waves generated by the tidal currents being deflected by the continental slope (as have been seen near the Southern California coast), and rising close to the surface because the thermocline becomes more shallow and often tilts upward in this region (Fig. 4). This view is mentioned because previous experimental studies have demonstrated the detectability of internal waves, due to the manner in which their currents affect the small-scale roughness [8]. Except for the December 14 flight, boundaries taken from the CV-990 were frequently obscured by cloud coverage. None of surface photographs showed any distinctive optical feature or foreign material at this location that might explain the radar observations. This negative photographic result would be consistent with the internal wave phenomena.

Another possibility is the presence of significant amounts of small-sized foreign material or debris which could be convected and aligned by the current. However, this condition might lead to a reduction in the local surface tension and roughness, which would then appear as a distinct depression in the radar cross section. Close examination of one image (accompanied by quantitative digital image scanning to infer a radar cross-section profile across this feature) reveals an oscillatory behavior, where the cross section ranged above and below the average value on the Gulf Stream. These features of the data, along with the absence of any visible (photographic) evidence, leave open the question of what type of phenomena is being detected here.

6. Interpretations Based on Surface Stress

The variety of observed cross-section effects suggests that several ocean phenomena may be responsible for the features seen on the strip chart record and the SAR images. It must be kept in mind that the modulation of radar echo is controlled primarily by the surface roughness, so that only those quantities that might influence this roughness must be examined. For example, the wave-wave interactions between long gravity and short gravity (and capillary) waves will produce effects with smaller spatial scales than are of interest in this analysis. The critical control of this surface roughness is the shear flow of winds close to the surface, to which the small Bragg-wavelength ocean waves are tightly coupled. This wind stress is known to be influenced by the mean wind several meters above the surface, any water current at the surface, and the air-sea temperature difference (especially under stable conditions). Aspects such as fetch and time scale for growth of waves of this size are believed to play a minor role in these cross-section measurements due to the time and spatial averaging inherent in this method. The discussion that follows will attempt to relate these quantities to the observed results, using known surface conditions and plausible ocean phenomena in this region.

The general question of why the Gulf Stream is always rougher than the water of the continental shelf water should be addressed in terms of the two most significant characteristics of this body: (1) it has a significant current distributed over a wide area that flows in a well-defined direction, and (2) its temperature is higher than the water on the continental shelf and is often higher than the overlying atmosphere.

The data shows that neglecting temperature and accounting only for the current magnitude and direction relative to the prevailing wind will not explain the observed cross-section changes. If the wind had a strong component antiparallel to the current, the friction velocity (and the radar cross section) on the Gulf Stream would be greater than it is on the stationary shelf water. Alternatively, for a wind component parallel to the current, the friction velocity on the Stream would be lower than on the shelf, implying that the shelf should have a larger cross section. Examination of the data shows that the shelf never had a greater cross section than the Gulf Stream. No changes in cross section can be correlated solely with wind direction changes for the five days described above. For example, on December 4, the winds were from the northeast, and on December 15 they were from the southeast, but larger cross sections on the Stream are clearly evident in the data for both days (Table 3). The conclusion here is that while the current velocity may influence the relative roughness between the Gulf Stream and the shelf, it cannot be assigned the dominant role.

TABLE 3. SURFACE INFORMATION AND TIMES OF OBSERVATION

Date	Time (GMT)	Station	Wind Speed, m/s	Wind Direction, deg	Air Temperature, °C	Sea Temperature in Gulf Stream, °C
Dec. 4	17:00:00	III	3	060	23.8	25.2
Dec. 4	20:00:00	III	4	080	25.3	25.2
Dec. 15	17:00:00	I	5	150	-	-

It seems fruitful to consider the state of knowledge of the dependence of wind stress on the air-sea temperature difference [9]. The emphasis in the literature on this subject is on the study of the growth of wind waves (large gravity) over large fetches, for long periods. The available evidence points conclusively to the importance of atmospheric stability, which depends on the vertical temperature gradient. Comprehensive field measurements indicate that when all other quantities are equal, a sea temperature larger than the air temperature (unstable conditions) causes the heights of waves generated to be greater, due to the higher drag coefficient of the surface.

Studies of experimental data carried out by Fleagle [9] lead him to conclude that the increase in wave height due to an air-sea temperature difference (unstable) is at the rate of 10% of the height per degree centigrade. Examination of our available surface-temperature information indicates that the sea temperature was never less then the local air (measured from the ship at Station III). On days such as December 4 and 6, moderate differences in temperature are evident (about 1 to 2 deg), consistent with the observation of larger cross sections on the Stream.

It should be emphasized that a nonneutral temperature condition alone cannot explain the cross-section variations, since a constant sea-surface temperature would yield the same cross section everywhere. If wind stress is the controlling factor, then it must be the temperature differences between the Gulf Stream and the shelf that account for the cross-section differences. Since surface temperature variations can be inferred from the satellite observations, some quantitative estimates of the variations of the drag (shear stress) coefficients, and the tangential stress of the wind on the sea due to thermal stratification can be made. Besides the temperature variations, the variation in the resultant velocity between the mean wind and local Gulf Stream current will also be considered in the surface stress calculation. These changes in wind stress can then be compared with the radar data.

It is customary to express the surface drag τ_0 of the wind at the surface in terms of the mean wind speed at a chosen reference height (10 m will be used in the following). This, then, defines the drag coefficient [10], C_{10}:

$$\tau_0 = (\text{air density}) \times C_{10} \times \overline{U}_{10}^2 \qquad (1)$$

$$C_{10} = (U^*/\overline{U}_{10})^2 \qquad (2)$$

U_{10} = mean wind speed at 10 m above the surface

U^* = friction velocity

For a fixed $\overline{U}_{10}$, any change in the vertical wind profile caused by temperature stratification will alter C_{10}. From these equations, it is evident that a change in C_{10} will also change the surface stress. Most data on C_{10} available in the literature is for neutral conditions. Approximate methods to take vertical gradients of temperature into account have been developed [11] and supported by experimental results.

This approximate theoretical development will be applied here to estimate the magnitude of the effects that were likely to occur during these Marineland Test flights. Since relative changes in wind stress are of interest (on and off the Gulf Stream) only the ratio of C_{10} at the measured air and sea temperatures relative to the value for a uniform temperature profile need be calculated. For the neutral condition, $(C_{10})_n$ depends primarily on the dynamic roughness, z_0, [10].

$$\left(C_{10}\right)_n = \frac{k^2}{\left[\ln\left(\frac{10 + z_0}{z_0}\right)\right]^2} = \left[\frac{(U_*)_n}{\overline{U}_{10}}\right]^2 \qquad (3)$$

For a slightly stratified condition, the approximate similarity theory solution for the heat flux advanced by Monin and Obukhov [10] yields

$$\frac{U_{10}}{U_*} = \frac{1}{\left[\left(C_{10}\right)_n\right]^{1/2}} + \frac{10\alpha\gamma}{kL} \qquad (4)$$

After some manipulation and insertion of the values for the constants α, k, and γ found in [10] and [11], the desired ratio is expressed as:

$$C_{10}/\left(C_{10}\right)_n = \left[1 - 1.24\,\frac{\Delta\theta}{\overline{U}_{10}^2}\right]^2 \qquad (5)$$

where

$\Delta\theta$ = the air temperature minus the sea temperature, °C

$\overline{U}_{10}$ = wind speed at 10 m above the surface, in m/s

It is readily seen that for a warmer sea $\Delta\theta < 0$ and $C_{10} > (C_{10})_n$. Also, the effect becomes weaker for a higher wind condition, where the instability due to thermal stratification becomes subordinate to the dynamic turbulence.

A more sophisticated and critical appraisal of the state of knowledge of the factors that affect the drag coefficient can be found in a report on the marine boundary layer by Cardone [12].

1. Surface Stress Implications for 04 December, 1975

The prime data set for these surface stress/radar backscatter comparisons is 04 December 1976, since there are VHRR thermal images before and after two independent radar observations. In particular, the VHRR data was obtained at 1300 GMT on December 4, and 0200 GMT on December 5, and the radar data was obtained on "Gulf Stream transits" at 1700 GMT and 2000 GMT on this day.

This thermal data is in the form of quantized sea-surface temperature levels (separated by approximately 1.1°C), each level representing the temperature within a 2-km square cell. This resolution is comparable to that of the radar cross-section data. Figure 10 shows the two dimensional surface-temperature distribution at 1300 GMT, where the lines represent boundaries between the quantized temperature areas. The surface latitude and longitude coordinates are superimposed on this information to permit the construction of a temperature profile along the same ground path traversed by the radar for comparison with the radar cross-section variations, and for inclusion in a stress profile calculation. This profile is seen in Figure 11. Three interesting properties are evident:

(1) The temperature difference between the Gulf Stream and the shelf water is substantial, typically 4°C, with some small areas being 5°C warmer than the shelf. The temperature gradients in the shelf waters are by no means in the same direction, although the average behavior is for the temperature to decrease as one gets closer to shore. The substantial irregularities of the boundaries that separate the areas of uniform temperature are seen in Figure 24.

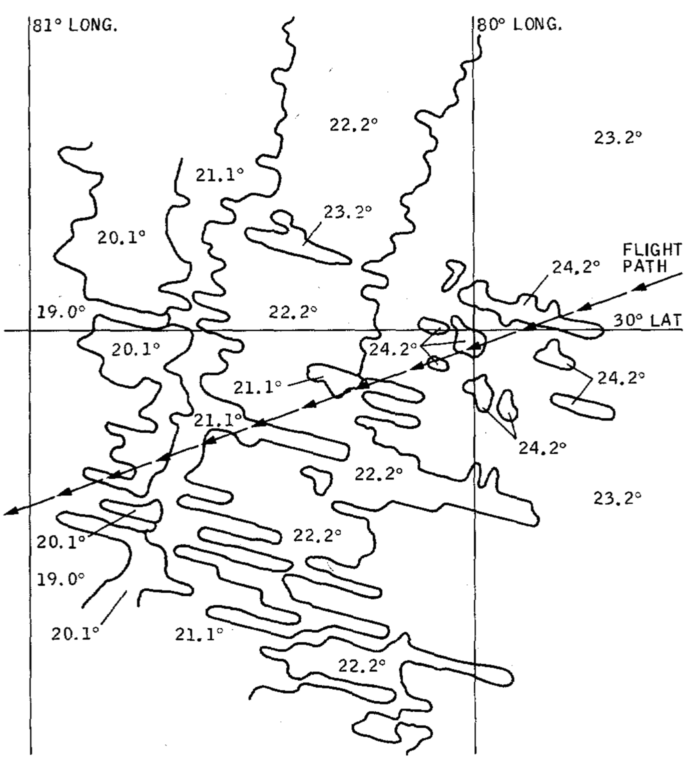

Fig. 10. Isotherms Inferred from Quantized Infrared Imagery December 4, 1975, 1300 GMT - Rev. No. 4807

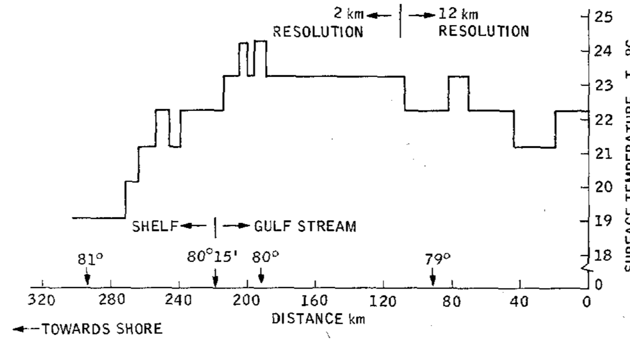

Fig. 11. Temperature Profile Along Gulf Stream Flight Path, December 4, 1975, 1300 GMT - Rev. No. 4807

In order to relate the radar cross section at this microwave frequency and incidence angle to the wind stress at the sea surface, this temperature information can be utilized in a theoretical calculation of the stress along the line of flight. As noted above, the magnitude of the drag coefficient is quite sensitive to any thermal stratification in the air, either stable or unstable. The wind speed (relative to the surface) also influences the drag coefficient, as well as being the dominant quantity in the total stress. Surface station instruments have recorded the wind speed and direction at the flight times of interest. The product of this drag coefficient and the square of the magnitude of the resultant vector velocity difference between the air and water surface (including the effect of the water current) equals the total stress. (See Appendix.)

This theoretical approach was followed, and a profile of sea-surface stress was calculated for comparison with the radar cross-section data. This included the temperature data of Figure 11, the known wind speed of 4 m/sec, and direction of 60° was combined with a northward Gulf Stream current. No timely observations of the Stream's structure or velocity were available for use in computing this surface stress. As an example of a "representative" shape, size, and current magnitude, the profile presented by Von Arx (Atlantis cruise No. 165, near latitude 38°, longitude 70° [5] was used in all the stress calculations presented herein. This embodies a width of 90 km, a maximum speed of 2.2 m/sec, and a western border at 80° 15', where the continental slope is steepest. The square root of the normalized stress is plotted in Figure 5(b), along with the radar cross-section profile that was measured about four hours later. The square root of the stress was plotted because previous aircraft measurements of the dependence of the cross section on the wind speed have shown it to be closer to a unity power law form (hence, square root of stress) than a square law dependence (linearly proportional to stress) [13].

The computed square root of surface stress and observed backscatter profiles have a striking similarity. The magnitudes of both are higher on the Gulf Stream relative to the cold shelf. Also, both levels increase as one travels toward the western edge from the east. In addition, a steep decline occurs where the current gradient is believed to be in the greatest. Furthermore, in the region on the eastern edge of the continental shelf where the current is very small, the cross section is still relatively high and correlates well with the higher stress resulting from the relatively higher temperature in this region.

A second data set on December 4 showed similar features. The second Gulf Stream transit was conducted at 2000 GMT, and a subsequent satellite photograph 6 hours later (at 0200 GMT, December 5) provided a sea temperature profile. These profiles are presented in Figure 6. Again, the length of the higher cross-section region extends twice as far as the width of the Gulf Stream, and with a steep decrease at the location where the current rapidly decays. Considering the six-hour time difference between these observations, the degree of agreement is considered satisfactory. Comparing the maximum and minimum magnitude levels reached by the measured cross section with the maximum and minimum levels of the square root of the stress, it appears that this value of the exponential power gives a good functional dependence for both data sets. A unity power law gives a poor fit.

2. Surface Stress Implications for 15 December, 1976

Further support for the preceding interpretation comes from the analysis of the data acquired during the first Gulf Stream transit on December 15 (Figure 8). This data was puzzling because the cross section on the western half of the Stream was (on the average) lower, as compared to the continental shelf, and to the eastern half of the Stream (which still had relatively higher roughness than the shelf). The radar cross section can be related to surface stress, only if one accounts for surface wind speed and sea-air temperature differences. The surface wind which was coming from the southeast produced a smaller relative velocity on the faster moving areas of the Stream, as compared to the slower current on the eastern half. Also, the higher temperature of the Stream increases the stress (and observed cross section) relative to the shelf. Unfortunately, cloud cover prevented the acquisition of satellite temperature information, but a crude model (based on the earlier temperature features seen on December 4) was assumed and combined with the Gulf Stream current velocity profile along with the measured wind information to compute a stress profile for comparison (Figure 8(b)). The general behavior of this theoretical curve agrees with the observed features noted above. The strong fluctuations in the radar data near the continental slope may be related to stronger temperature variations than those seen on December 4. This is suggested because a satellite infrared image taken on December 16 (24 hours later) shows a very intense, small eddy activity at this side of the Gulf Stream that may have existed at the time the radar observations were made.

7. Conclusions and Recommendations

The foregoing results demonstrate that the imaging radar measures an average radar cross section of the ocean surface that is related to surface stress. This relationship complements the Seasat-A SAR's primary objective of observing the directional spectrum of ocean waves. The directional alignment of the radar line-of-sight played an important role in the interpretation of the radar cross-section observations. When several different directions were examined, the radar backscatter properties showed that the wind-driven, small gravity waves were aligned with the average wind direction. The observations of the Gulf Stream in this experiment provided an excellent opportunity to study the combined effects of wind magnitude and direction, of surface-current and of sea-air temperature differences on the surface roughness. The analysis carried out in this report, along with the radar and surface data presented, is in close qualitative agreement. While additional surface and related supporting information could be utilized (and would be welcome), the general behavior of the measured results can be explained with well-known phenomena that, heretofore, have been impossible to witness with as comprehensive and sensitive measurement as this. Prior to this experiment, very little experimental evidence existed to demonstrate the relationship and dependence of roughness on sea-surface temperature and air-temperature profiles. This fact could have implications for the interpretation of other microwave sensor systems, such as the radiometer and scatterometer.

Because of the ability of the microwave energy to penetrate clouds, the results described here could lead to a system for monitoring Gulf Stream current variations (given supporting satellite-temperature information) or they could be used for the detection of temperature variations (with a higher degree of spatial resolution than a satellite radiometer) in regions where current and other surface dynamic features are known to be sufficiently small.

References

1. Moskowitz, L.I., "The Feasibility of Ocean Current Mapping via Synthetic Aperture Radar Methods," Proceedings of the American Society of Photogrammetry, Part II, pp. 760-771, 1973.

2. Parsons, C.L., "An Observational Study of σ° variations in the Vicinity of the Gulf Stream," in SKYLAB S-193 RADAR ALTIMETER EXPERIMENT ANALYSIS AND RESULTS, G.S. Brown, Ed., CR-2763, Feb. 1977.

3. Shemdin, O.H., Blue, J.E., and Dunne, J.A., SEASAT-A Surface Truth Program: Marineland Test Plan, Memo 622-6, November 1975, (JPL internal document).

4. Wright, J.W., "A New Model for Sea Clutter," IEEE Trans. Antennas Prop., AP-16 (No. 2), 1968, pp. 217-223.

5. Von Arx, W., Introduction to Physical Oceanography, Addison-Wesley, 1974.

6. Weissman, D.E. and T.W. Thompson, "Preliminary Study of the Radar Cross-Section Variations at the Western Boundary of the Gulf Stream," SEASAR TN-7, August 4, 1976.

7. Thompson, T.W., JPL Radar Operations Report, Marineland/GASP Test Series, 25 November to 16 December 1975, Technical Memorandum 622-13, Jet Propulsion Laboratory, Pasadena, Calif., April 1, 1976, SEASAT TN-8.

8. Elachi, C., and J.R. Apel, "Internal Wave Observations made with an Airborne Synthetic Aperture Imaging Radar," Geophys. Res. Letts., Vol. 3, No. 11, 1976, P. 647.

9. Fleagle, R.S., "Note on the Effect of Air-Sea Temperature Difference on Wave Generation," Transactions of the American Feophysical Union, Vol. 37, No. 3, pp. 275-277, June 1956.

10. Roll, H.U., Physics of the Marine Atmosphere, Academic Press, New York, 1965.

11. Deacon, E.L., "Aerodynamic Roughness of the Sea," Journal of Geophysical Research, Vol. 67, No. 8, pp. 2167-3172, 1962.

12. Cardone, V.J., "Specification of the Wind Distribution in the Maring Boundary Layer for Wave Forecasting," Report TR-69-1, New York University School of Engineering and Science, March 1970 (Available as DDC no. AD702).

13. Daley, J.C., An Empirical Sea Clutter Model, Memorandum Report 2668, Naval Research Lab., Washington, D.C., October 1973.

14. Uchupi, E., Map Showing Relation of Land and Submarine Topography, De Soto Canyon to Great Bahama Bank, Department of Interior, United States Geological Survey, Miscellaneous Geologic Investigations Map I-475, 1966.

Appendix - Surface Stress Calculation

Surface Stress = (Air Density) x (Drag Coefficient) x (Magnitude of Relative Velocity at 10 Meters Above Surface)^2

$$\tau_o = \rho C_{10}\, U_{10}^2$$

$$C_{10} = (C_{10})_n \left[1 - \frac{1.24\,(T_a - T_s)}{\overline{U}_{10}^2}\right]^2$$

C_{10_n} = Drag coefficient under neutral (uniform) temperature conditions

T_a = Air Temperature - °C

T_s = Surface Temperature - °C

$\overline{U}_{10} = |\vec{U}_w - \vec{U}_c|$ = Magnitude of vector difference between wind and surface current

$\vec{U}_w$ = Wind Velocity Vector

$\vec{U}_c$ = Surface Current Velocity (Assumed to be in northerly direction at all points)

Square Root of Normalized Stress

$$= \sqrt{\frac{\tau_o}{\rho (C_{10})_n\, |U_w|^2}}$$

$$= \left[1 - \frac{1.24\,(T_a - T_s)}{U_{10}^2}\right] \times \frac{\overline{U}_{10}}{U_w}$$

$$= 1 \text{ when } \vec{U}_c = 0 \text{ and } T_a = T_s$$

ACKNOWLEDGEMENT

The authors thank all members of the Marineland Test Team for their support. The Medium Altitude Mission Branch, NASA Ames Research Center provided its usual invaluable assistance during the flight operations. Several members of the Space Science Division at the Jet Propulsion Laboratory provided many useful inputs to the analysis. And as mentioned in the text, a vital data set was the infrared surface temperatures provided by Dr. Richard Legeckis of NOAA-NESS.

Work performed at the Jet Propulsion Laboratory is one phase of the research carried out under Contract NAS 7-100 to the National Aeronautics and Space Administration.